

Measuring the matter distribution within $z = 0.2$ cluster lenses with XMM-Newton

P. B. Marquet^{1,2}, S. Bardeau², O. Czoske², H. Ebeling³, J. P. Kneib^{2,4}, R. Sadat², and I. Smail⁵

¹IA.S., Université Paris-Sud, Bât. 121, F-91405 Orsay cedex, France

²L.A.T., Observatoire Midi-Pyrénées, 14 av. Edouard Belin, F-31400 Toulouse, France

³Institute for Astronomy, University of Hawaii, 2680 Woodlawn Drive, Honolulu, HI 96822, USA

⁴Caltech-Astronomy, MC 105-24, Pasadena, CA 91125, USA

⁵Institute for Computational Cosmology, University of Durham, South Road, Durham DH1 3LE, UK

ABSTRACT

We present an analysis of 7 clusters observed by XMM-Newton as part of our survey of 17 most X-ray luminous clusters of galaxies at $z \approx 0.2$ selected for a comprehensive and unbiased study of the mass distribution in massive clusters. Using the public software FTTOOLS and XMM SAS we have set up an automated pipeline to reduce the EPIC MOS & pn spectro-imaging data, optimized for extended sources analysis. We also developed a code to perform intensive spectral and imaging analysis particularly focussing on proper background estimate and removal. XMM-Newton deep spectro-imaging of these clusters allowed us to fit a standard model to their gas emission profiles as well as a standard MEKAL emission model to their extracted spectra, and test their inferred characteristics against already calibrated relations.

INTRODUCTION

Being the most massive gravitationally bound objects in the Universe, clusters of galaxies are prime targets for studies of structure formation and evolution.

Of particular interest are the most X-ray luminous clusters. Indeed, it has been convincingly demonstrated that high X-ray luminosity is a reliable indicator of cluster mass (e.g. Allen, 1998). Therefore, X-ray selected clusters samples (e.g. Ebeling et al., 1996) are the best choice for undertaking representative studies of the mass distribution in massive, X-ray luminous clusters. In particular, as they are easily detected out to very large redshift, we can hope to probe cluster evolution back from early epochs. However, X-ray luminosity is also sensitive to the presence of cooling flows, mergers and non-thermal effects, thus the Luminosity-Mass and Temperature-Mass relation needs to be clearly understood before any strong assertion is made on cluster evolution (Smith et al., 2003). Proper mass estimate is likely to arise only by combining multiwavelength observations of clusters of galaxies: namely strong and weak lensing observations (Smith et al., 2001), velocity distribution and dynamics of the cluster galaxies (in a similar way as in Czoske et al., 2001) and through accurate, spatially resolved X-ray temperature measurements as we are concentrating on here.

Following this premise, we are conducting a survey (Table 1) of the most X-ray luminous clusters ($L_{X(0.1-2.4\text{ keV})} \approx 8 \times 10^{44} \text{ erg s}^{-1}$) in a narrow redshift slice at $z \approx 0.2$, selected from the XBACS (X-ray Brightest Abell-type Clusters Sample; Ebeling et al., 1996). As XBACS is restricted to Abell clusters (Abell, Corwin & Olowin, 1989), it is X-ray flux limited but not truly X-ray selected. However, a comparison with the X-ray selected ROSAT BCS (Brightest Cluster Sample, Ebeling et al., 2000) shows that

75% of the BCS clusters in the redshift and X-ray luminosity range of our sample are in fact Abell clusters. Hence, our XBACS subsample is, in all practical aspects, indistinguishable from an X-ray selected sample.

Table 1. Our cluster list sorted by right ascension. Redshift, Hydrogen column density, flux and luminosity (columns 3 to 6 resp.) are quoted from the XBACS updated database. Out of these 17 clusters, 8 have HST/WFPC2 observations performed (as part of cycle 8 [ID :8249, P I K neib]); 3 only have a shallow HST observation through a snapshot survey (8301 & 8719 programmes, P I E dge); 2 have not yet been observed with HST; the remaining 4 having archival data. Moreover, 11 have been observed in 1999/2000 with the wide field CFH12K camera ([Czoske et al., 2003]). The last column shows the effective exposure duration (after ares removal) for clusters already observed by XMM-Newton (resp. MOS and pn instruments), or quote the priority level within our proposal for those not yet observed.

ID	J2000	J2000	z	N_H 10^{20} cm ²	$f_{x\text{bacs}}$ 10^{12} cgs	$L_{x\text{bacs}}$ 10^{44} erg=s	HST cycle	CFH semester	XMM-Newton ks (MOS/pn)
A 68	00 37 06	+ 09 09 20	0.2546	4.77	5.55	14.90	8249	99-II	22/10
A 115	00 55 55	+ 26 22 14	0.1971	5.39	8.99	14.57	-	-	C
A 209	01 31 53	13 36 47	0.2060	1.56	7.55	13.38	8249	99-II	17/11
A 267	01 52 41	+ 01 00 43	0.2300	2.84	6.21	13.67	8249	99-II	17/12
A 383	02 48 03	03 31 04	0.1871	4.06	5.50	8.09	8249	99-II	25/07
A 773	09 17 52	+ 51 43 38	0.2170	1.34	6.36	12.50	8249	-	15/15
A 963	10 17 03	+ 39 02 56	0.2060	1.40	5.78	10.27	8249	99-I	24/16
A 1423	11 57 17	+ 33 36 39	0.2130	1.66	5.22	9.92	8719	-	C
A 1682	13 06 49	+ 46 33 35	0.2260	1.36	5.44	11.59	8719	-	C
A 1689	13 11 29	01 20 31	0.1840	1.80	14.60	20.64	6004	00-I	A O 1 J H ughes
A 1763	13 35 19	+ 40 59 56	0.2279	0.84	6.54	14.13	8249	99-II	observed
A 1835	14 01 02	+ 02 52 03	0.2528	2.24	14.58	38.24	8249	99-I	P V (27/23)
A 2111	15 39 42	+ 34 25 03	0.2290	2.07	5.01	10.97	-	-	C
A 2218	16 35 54	+ 66 13 00	0.1750	3.20	7.3	17.99	5701, 8500	00-I	G T M Tumer
A 2219	16 40 20	+ 46 42 27	0.2281	1.73	9.23	19.89	6488	00-I	G T M Tumer
A 2261	17 22 27	+ 32 07 53	0.2240	3.36	8.72	18.15	8301	-	A O 1 J H ughes
A 2390	21 53 37	+ 17 41 45	0.2310	6.70	9.50	21.25	5352	00-I	G T M W atson

THE ANALYSIS PIPELINE

As to the version 5.2 of the official XMM-Newton data analysis software (XMM SAS), the extended sources could not be handled properly, regarding the background subtraction and vignetting corrections. The development of methods, where weights are applied to events according to their energies and positions as well as calibration data so as to correct the event list as if the instrument response were uniformly identical to the on-axis response, started as soon as 2001 ([Amaud et al., 2001, Majerowicz et al., 2002, Marty et al., 2002, Marty et al., 2003]). We concentrated on our side to embedding these algorithms into an environment capable of pipeline processing a series of data from clusters of galaxies observations. Indeed, the manual operation of XMM SAS (using either external correction routines or integrated algorithms from versions 5.3 and later) is extremely time-consuming: several days for each dataset.

Thanks to our pipeline, we reduced the required time down to less than 10 h per dataset, adding a working day for eye-inspection of the full sample results and another for compilation and final manual calculations.

This pipeline integrates the latest calibration data from the EPIC consortium as well as specific routines written in IDL and XSPEC environments. It is fully configurable to allow eye-inspection and partial or total re-runs if needed. It is extensively detailed by [Marty et al., 2003], but useful information about "blank" and "dark" fields (for background estimation and subtraction) are also respectively given by [Lumb et al., 2002, Marty et al., 2002]. The general processing scheme is the following:

- re-process each cluster raw data to account for latest calibration knowledge;
- re-project "blank" and/or "dark" data onto telescope aspect solution used for each cluster;
- extract valid events within good-time-intervals (to reject noise and proton ares);
- detect and mask out spurious components (field sources and remaining bad pixels);
- weight the events according to calibration data;
- find the best cluster centroid;
- process radial brightness profiles and fit a standard model convolved by the instrument PSF;
- process full maps in physical flux units and adaptively smooth according to PSF description;
- process spectra and call XSPEC for fitting (global for the mean temperature, annuli for the profile);
- compute hardness maps and derive another temperature profile.

THE PIPELINE RESULTS

Surface brightness profiles

The core radius R_c , power index α , normalization f_0 and background constant BKG are coming from the standard β -model fitting. Note that the surface brightness profiles have been extracted between 0.3 and 6.3 keV, logarithmically rebinned to enhance their signal-to-noise ratios and that the inner 40 arcsec of each cluster profile have been ignored for the fit so as to avoid fitting any emission excess, associated for example to a cooling flow. The background subtraction concerned only the instrumental component so that the BKG constant is a measure of the sky X-ray emission background. The β -models are convolved by the instrument PSF before fitting.

The $R_{1\sigma}$ parameter is a measure of the radius inside which the cluster signal-to-noise ratio is greater than 1. The F_X (data) and F_X (model) parameters then are the integrated fluxes within this detection limit radius, from the data and from the best fit model; in each case, these fluxes are cleaned from the sky background component; the difference between them thus shows the contribution of any excess emission.

Surface brightness maps

Surface brightness maps that have been produced in the same energy band during the pipeline analysis are not presented herein, because of room restrictions and because they are not necessary for the following calculations. However, they may be found on the internet¹ if so desired.

Spectral analysis

Spectra are extracted in the 0.2 to 12.0 keV band and rebinned according the Poisson statistics requirements (at least 25 net counts per bin). They are background subtracted from both instrumental components (estimated using the "closed" data) and sky components (from a spectrum extracted in a peripheral annulus of each dataset, between the 600 and 800 arcsec radii) and then fitted against the TBabs MEKAL photo-absorption and bremsstrahlung models.

The redshifts z and hydrogen column densities N_H have been respectively fixed to the same optical redshift references as used in the original XBACS database, and to the weighted means of the N_H measurements from the [Dickey & Lockman, 1990] database included within 1 deg of the cluster center. The resulting temperatures kT , abundance relative to solar composition and normalization S_0 are then reported. These measurements come from spectra extracted inside a circle of 400 arcsec radius, and hence integrate any central excess emission; that is why temperatures may appear a bit low.

Direct temperature profiles

Spectra have also been extracted within 40 arcsec-wide concentric annuli following the same algorithm than for global spectra. Fitting them using the same XSPEC settings hence led to a direct measure of the temperature profile of each cluster. However, no PSF correction have been applied from one annulus to another thus probably leading to a general underestimation in the fitted temperatures, specially toward the center (Markevitch, 2002).

A last spectrum has been extracted and fitted, in the same region than that used for the β -model fitting, i.e. an annulus starting at 40 arcsec and extending upto the arbitrary limit of 400 arcsec. This allows to compare between the global temperature with the one found outside the core region, which may host a cooling flow.

Intrinsic parameters calculation

The luminosity distance D_L and 1 arcsec equivalent length $R_{1''}$ at the cluster position are deduced from the cluster redshift z and the default cosmology ($\Omega_0 = 1$, $\Omega_m = 0$ and $H_0 = 50 h_{50}$ km/s/Mpc).

The virial radius R_V has been identified with the distance r_{200} from the cluster center where the mean enclosed overdensity equals 200, as calibrated upon the measured X-ray temperature by [Evvard et al., 1996].

The X-ray luminosity L_X was integrated between our XMM-Newton energy bandwidth (0.3 - 6.3 keV) within the virial radius defined above. We applied a numerical bolometric correction to deduce the absolute luminosity L_X (bol).

¹Only compiled on ftp://www-station.ias.u-psud.fr/pub/epic/HiLx/2002Marty_santiago_poster.jpg at the moment, but individual maps will soon be available in the same ftp directory.

The galaxies velocities dispersions w_b and w_{\perp} have been reprinted from two weak lensing analysis, respectively from NOT/ALFOSC and UH8k detectors (Dahle et al., 1990), and CFHT12k instrument (Bardeau & Kneib, 2003). The corresponding parameters were computed according to the relationship with them measured X-ray temperature in the isothermal hydrostatic equilibrium case (Cavaliere & Fusco-Femiano, 1976)

The electronic density $n_e(0)$ at the center of the cluster has been estimated using the standard isothermal model equations (Cavaliere & Fusco-Femiano, 1976) and the previously measured X-ray temperature and luminosity. By integration within the virial radius defined above, we also estimated the cluster gas mass. Finally, the total virial mass has been deduced from two different calibrated relations upon the measured X-ray temperature (M_B and M_T resp. from Cavaliere & Fusco-Femiano, 1976, Amaud & Evrard, 1999) as well as from the virial theorem relation upon the galaxies velocities dispersion (M_V from the w_b defined above, except for A 773 for which we used w_{\perp}). The gas fraction f_g simply is the ratio of the gas mass to the total mass (we chose M_B as the isothermal reference).

DISCUSSION

All analysed clusters show an excess in central brightness that seems correlated with the presence of a very bright central galaxy in optical images. They hence are all candidates for cooling flow hosts, but A 267 and A 383 temperature profiles do not exhibit significant cooling cores. In addition, all clusters but A 1835 tend to follow the universal temperature profile calibrated by Loken et al., 2002 (Figure 3), radii being rescaled either to core radius or virial radius natural units, with a declining slope toward the edges. They are also very close to the Degrandi & Molendi, 2002 polytropic interpretation of their Beppo-SAX observed clusters data, which show slopes more horizontal at high radii for those hosting a cooling flow than for non-cooling flow specimens, although our sample does not present a steeply cooling core in average.

If the problem of the cooling core may be bypassed by using only outer regions for temperature and model fitting, these declining profile still questions the hypothesis of isothermality followed throughout this first analysis. Nevertheless, we expect from the general good agreement of the different mass (Figure 2) and parameters estimations that our optical (CFHT12k) and X-rays (XMM-Newton) measurements are still both quite consistent with the isothermal model. But we note also that all calculations rely on a virial radius that has been estimated using a relation based on the isothermal hypothesis; that illustrates the need for another independent estimator of this radius. Even the clue given by the temperature profiles (Figure 3), that seem to indicate that the virial radius is about 10 times the core radius, is not so helpful if models fitted to either optical or X-ray data still rely upon isothermality.

We plotted a temperature-luminosity logarithmic diagram (Figure 1) for our subsample and compared it to the model proposed by Amaud & Evrard, 1999]. We observe that these clusters are indeed well co-aligned but following a shallower slope. A 209 seems to depart from this alignment, as well as A 1835 in a very significant manner. We also compared a temperature-velocity dispersion diagram with the model from Girardi et al., 1996] and found it to be very close to the lower 90% confidence level boundary, with again the exception of A 1835.

Finally, the temperature-mass diagram is remarkably consistent with a mean power index of 1.576, while the gas mass fraction seems to average about 10% except again for A 1835, as well as A 209 and A 773.

CONCLUSIONS & PERSPECTIVES

While early XMM-Newton observations (Amaud et al., 2001, Majerowicz et al., 2002) did not confirm declining temperature profiles as seen by late ASCA observations (Markevitch et al., 1998) and Beppo-SAX (Degrandi & Molendi, 2002, Loken et al., 2002), we find in the present analysis of 7 XBACS clusters that 6 of them do follow this kind of polytropic model. The seventh, A 1835, systematically departs from the average in all diagrams (temperature-mass, temperature-luminosity), which confirms the rather complicated nature of its internal dynamics (Majerowicz et al., 2002).

However, we still are working toward the comparison of these emission weighted temperature profiles, that have been obtained without correction for PSF and may thus have been underestimated (Markevitch, 2002), with profiles built on the basis of hardness ratio maps, that may be adaptively handled to account for the PSF and binned between concentric isophotes rather than concentric annuli to adapt to non-spherical morphologies. Also, more work is intended so as to derive accurate error bars on each diagram, and attempt to estimate the virial radii from independent optical datasets.

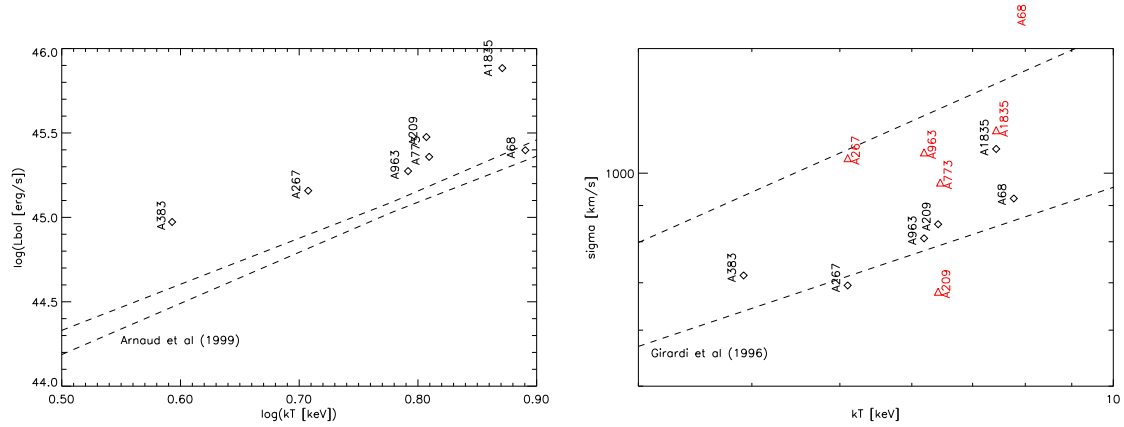


Fig. 1. Left: temperature-luminosity diagram as compared to the 90% confidence level range from [Arnaud & Evrard, 1999] model. Right: temperature-velocity dispersion diagram as compared to the 90% confidence level range from [Girardi et al., 1996] model (diamonds show values from [Bardeau & Kneib, 2003], triangles from [Dahle et al., 1990]).

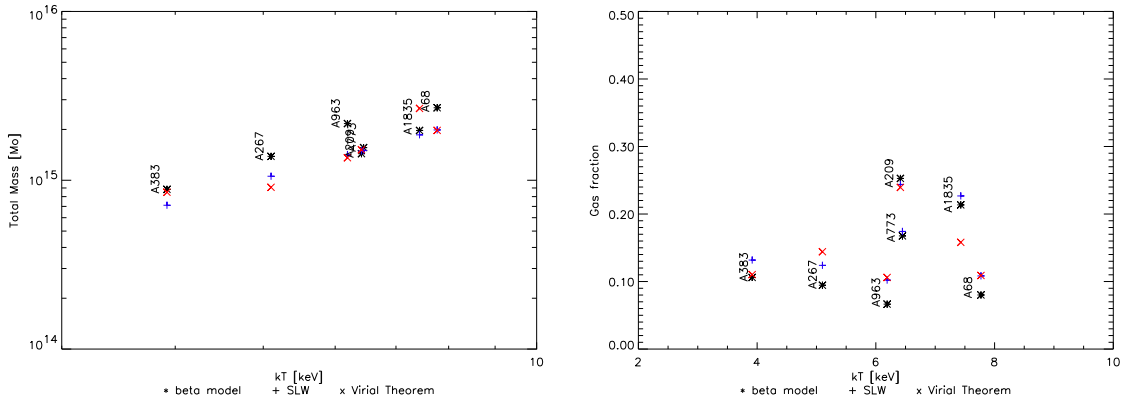


Fig. 2. Left: temperature-mass diagram, for different mass estimators, showing a mean power index of 1.576. Right: gas mass fraction, for the same estimators, as a function of the X-ray temperature.

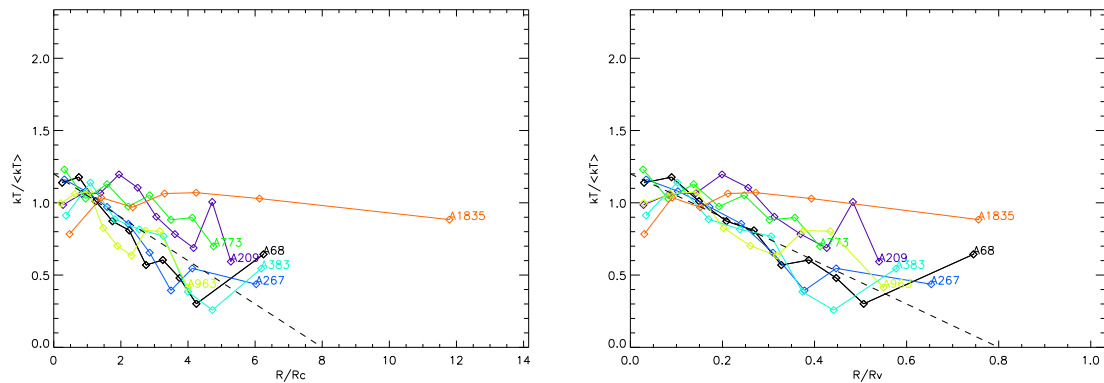


Fig. 3. Temperature profiles with radius rescaled either to core radius or virial radius units. The dashed line stands for the average slope in the central part of the polytropic simulation of [Loken et al., 2002].

